SAND2018-13219R

SAND2017-XXXX R

LDRD PROJECT NUMBER: 206536

LDRD PROJECT TITLE: Testing the possibility of magnetic domain imaging based on circular & linear dichroism using photoemission electron microscopy

PROJECT TEAM MEMBERS: Taisuke Ohta, Guild Copeland

ABSTRACT:

In recent years, an increasing number of memory and spintronic devices have been developed exploiting the combination of ferromagnetic (FM) and anti-ferromagnetic (aFM) materials. Consequently, magnetic imaging based on continuous-wave (CW) ultraviolet (UV) (λ=266nm and longer wavelength) photoemission electron microscopy (PEEM) is gaining considerable attention due to the possibility of determining magnetizations for FM and aFM materials with 10 nm lateral resolution at video rate image acquisition. This PEEM-based approach exploits the polarization-dependent photoemission yield, which is subject to the polarization vector and the FM or aFM magnetization direction. Because of this unique attribute, magnetic imaging using PEEM when coupled to a laser with multiple illumination geometries allows for characterizing in-plane and out-of-plane magnetizations. This concept, however, has not been tested using a deep-UV laser (λ=213nm), which has a much broader application space than the longer wavelength excitation used in previous reports. The purpose of this project in FY17 was to show the proof-of-concept of magnetic circular dichroism (MCD)-PEEM imaging using a λ=210nm pulsed laser. Our results demonstrated the feasibility of in-plane and out-of-plane magnetic imaging with the limitations in the lateral resolution, data acquisition time, and signal-to-noise ratio anticipated for using a pulsed laser of moderate power. The project goal for FY18 is to construct the automated polarization-controlled data acquisition, and to establish the new lab facility in anticipation of acquiring a state-of-the-art high-power 213nm CW laser, planned to be installed in FY19. We successfully demonstrate the former by measuringdielectric stacks with polarization-dependent photoemission yield. Extrapolating from our result, we conclude that the capability of PEEM-based magnetic imaging using a CW deep UV laser could be a potential game-changer for scientific investigations and technological developments of magnetic materials and spintronic devices. In addition, polarization controlled PEEM imaging shows the potential for ellipsometry imaging of embedded nanomaterials exploiting their subtle differences in optical constants with respect to their surrounding dielectrics.

INTRODUCTION:

With the emergence of spin-based devices (or spintronics), knowledge of magnetic domain behavior, spin-carrier dynamics, and energetics are of great importance from both scientific and technological points of view. Various approaches have been proposed and applied for magnetic imaging. As illustrated for ferromagnetic (FM) imaging in Table 1, each approach has notable

Sandia National Laboratories is a multimission laboratory managed and operated by National Technology and Engineering Solutions of Sandia LLC, a wholly owned subsidiary of Honeywell International Inc. for the U.S. Department of Energy's National Nuclear Security Administration under contract DE-NA0003525.

characteristics, and yields different kinds of information because each approach makes use of a dissimilar probing mechanism of magnetic information. To date, the approaches most commonly used are Kerr microscopy and Magnetic Force Microscopy (MFM) presumably due to the wider applicability and availability of these instrumentations. One significant shortcoming common in these two approaches is the lack of sensitivity to the direction of magnetization, which is an important component in the ability to characterize ever downsizing magnetic devices.

Among various experimental approaches for FM imaging, ones that allow the detection of magnetization direction include Scanning Electron Microscopy with Polarization Analysis (SEMPA), Spin-Polarized Low-Energy Electron Microscopy (SPLEEM), and X-ray Magnetic Circular Dichroism Photo Emission Electron Microscopy (XMCD- PEEM). Recently, PEEM coupled to continuous wave (CW) laser of ultraviolet wavelengths is gaining considerable attention due to the possibility of determining in-plane and out-of-plane magnetization with 10 nm lateral resolution and potentially video-rate imaging. This new approach relies on the dependence of the photoelectron emission yield (or simply photoemission yield) on the FM magnetization direction and the polarization vector of the incident circular polarized light, hence coined as magnetic circular dichroism (MCD). Until recently, commercially available CW lasers have been limited to $\lambda \geq 266$nm, which results in very low photoemission yield for the majority of materials, severely limiting the application of this approach.

The situation has been changing over the last few years, as CW lasers with shorter wavelength (λ=193nm, 213nm) and sufficient power are becoming available. Such short wavelength lasers allow PEEM measurements on practically any material, and potentially enable the control over the probing depth due to the steep dependence of the electron mean free path on the electrons' kinetic energy. What had not been shown before FY17 was a proof-of-concept that circularly polarized light with λ=193nm or 213nm can produce magnetic contrasts using PEEM. To verify this hypothesis, we proposed to conduct the proof-of-concept measurements using a λ=210nm pulsed laser with polarization control. The successful proof-of-concept measurements in FY17 allowed us to determine the viability of FM imaging using PEEM coupled to a deep UV laser for studying a wide class of magnetic materials and spintronic devices.

Table 1 State-of-the-art magnetic imaging approaches for ferromagnetic domains. Sited from W. Kuch, Magnetic Imaging, Lect. Notes Phys. 697, 275–320 (2006), modified to include UV MCD-PEEM approach. Faces with expressions illustrate the applicability, appropriateness, or superiority of the approaches. Columns refer (from left to right) to resolution, image acquisition speed, type of imaging (parallel imaging or scanning), sensitivity to applied magnetic fields, type of depth information (surface based or transmission), information depth (path length for exponential weighting for surface based techniques, maximum sample thickness for transmission techniques), possibility to obtain depth selective information. Acronyms for some approaches are as follows. SEMPA: Scanning Electron Microscopy with Polarization Analysis. SPLEEM: Spin-Polarized Low-Energy Electron Microscopy. XMCD- PEEM: X-ray Magnetic Circular Dichroism Photo Emission Electron Microscopy. UV MCD- PEEM: Ultraviolet Magnetic Circular Dichroism PEEM. M-XTM: Magnetic X-ray Transmission Microscopy. MFM: Magnetic Force Microscopy. Sp-STM: Spin-Polarized Scanning Tunneling Microscopy.

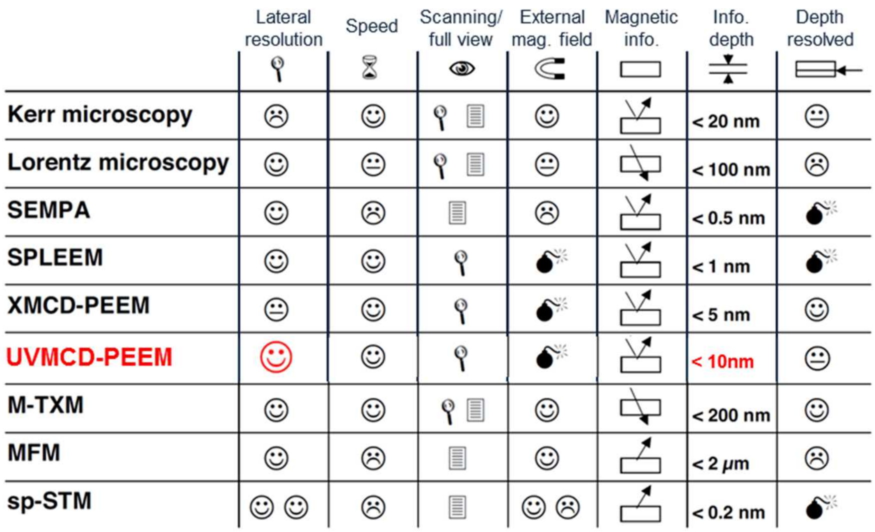

In contrast to FM imaging, imaging of anti-ferromagnetic (aFM) domains is much less explored due to the lack of an appropriate microscopy approach. Among the short list of approaches, X-ray Magnetic Linear Dichroism (XMLD)-PEEM and more recently, Scanning Probe Microscopy (SPM)-based approaches are two well-known contenders. Because many recently developed spintronic devices exploit the combination of FM and aFM materials, there is a compelling need to develop imaging approaches that are capable of the coincident-site FM and aFM imaging. To this end, an ultraviolet (UV) photoemission electron microscopy (PEEM) is a viable option because of the possibility to switch between FM and aFM imaging by controlling the illuminating light between circular and linear polarization. Extending our successful demonstration of FM imaging using UV-PEEM in FY17, we propose to construct an automated polarization-controlled data acquisition system in FY18. In addition, our goal is to establish the new lab facility in anticipation of acquiring a state-of-the-art 213nm CW laser, which is planned to be installed in early FY19. Here we report successful execution of the above-mentioned two objectives.

DETAILED DESCRIPTION OF EXPERIMENT/METHOD:

The proposed work includes two major tasks: (1) establishing the new lab facility in anticipation of acquiring a state-of-the-art high-power 213nm CW laser, and (2) constructing the automated polarization-controlled data acquisition.

The laboratory space in building 897/room B212 was significantly modified in order to accommodate the state-of-the-art high-power 213nm CW laser. We ordered the laser in mid-FY18, and plan for the manufacturer to install in early FY19. The laboratory now has an additional optical table (4’ x 8’), shelves for electronics, electrical outlets, and ultraclean nitrogen gas supply. Most of the optics to deliver the 213nm CW coherent light to our existing LEEM-PEEM instrument including the polarization controlling optics will be shared with the existing λ=210nm ultrafast pulsed laser described in the following.

The existing λ=210nm ultrafast pulsed laser is based on frequency quadrupling (HarmoniXX, APE Angewandte Physik & Elektronik GmbH) of the titanium sapphire (Ti:S) laser (Mira 900, Coherent Inc.), coupled to low energy electron microscope (LEEM) (LEEM III, ELMITEC Elektronenmikroskopie GmbH) operated as a PEEM. The Ti:S laser operates at 78MHz repletion rate to maximize the signal-to-noise ratio of PEEM images, while using a relatively low power to avoid the space charge within the electron optics of the LEEM. Figure 1 shows the schematic illustration of the LEEM setup equipped with light sources.

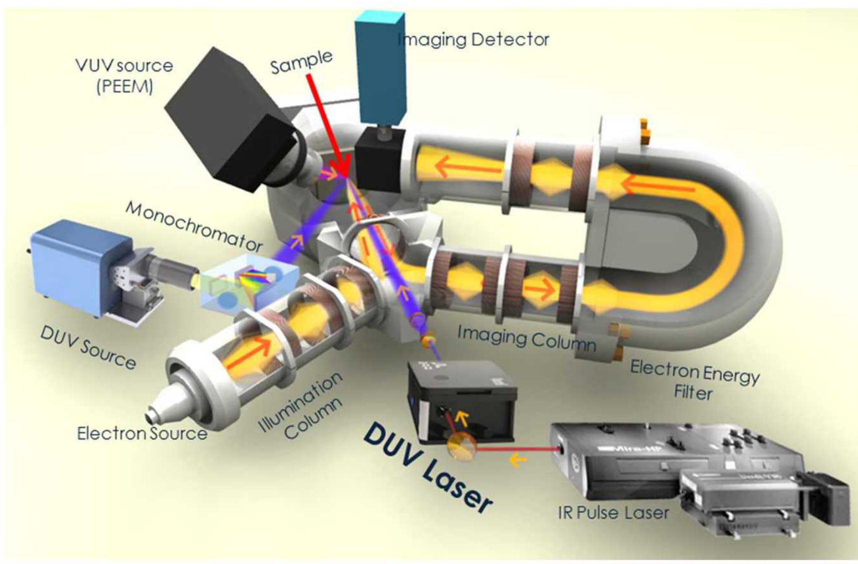

Figure 1 Schematic illustration of the LEEM setup equipped with three light sources. The optical path of the deep UV laser shown in the lower-right side of the illustration was modified for this project. The purple and red rays depict deep UV (DUV) or vacuum UV illumination, while yellow paths illustrate the electron trajectories through the electron optics of the LEEM.

In FY17, we constructed two laser beam lines, one with a normal incidence and another with a grazing incidence, to realize the in-plane and out-of-plane FM imaging. The two beam lines are depicted by the blue dash arrow (normal incident) and the red solid arrow (grazing incident) in the lower illustration of Fig. 2. The incident angle of the grazing beamline is 74° set by the available view port directed toward the sample position. We focus the light in the normal incident beamline using fused silica lenses, and in the grazing beamline using parabolic mirrors, both with no anti-reflective coating to avoid unwanted, uncharacterized absorption of deep UV light.

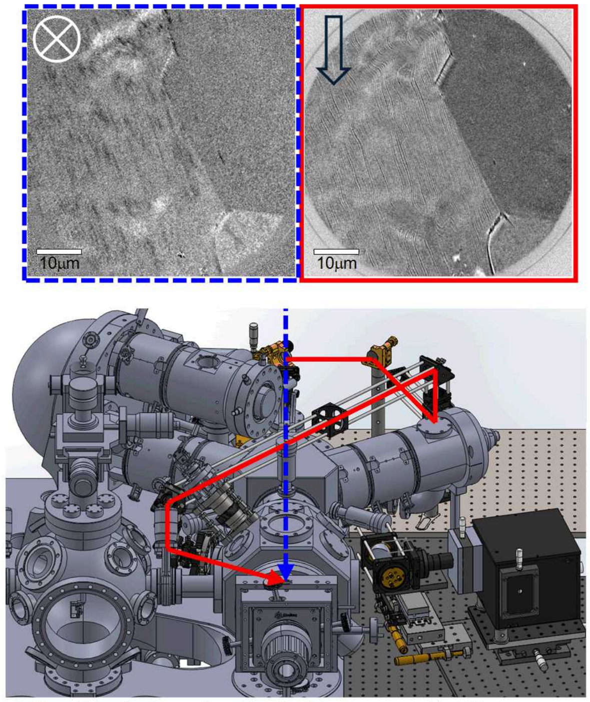

Figure 2 (Upper part) Representative in-plane and out-of-plane magnetization maps, and (lower part) drawing of the LEEM equipment with a normal (blue dash line) and a grazing (red solid line) incident beam lines constructed for this project. The sample was a cobalt film deposited on polycrystalline nickel as described in the results section. The out-of-plane (upper left) and in-plane magnetization (upper right) maps are acquired using a normal incident (blue dash arrow) and grazing incident (red solid arrow) illuminations depicted in the drawing of the LEEM equipment.

For the work conducted in FY18, we used linearly polarized light generated using a half wave plate for λ=213nm (Kogakugiken Corp.). we controlled the light polarization direction using a rotation stage (Thorlabs, Inc.). No additional polarizer was used to condition the incoming light because the output light of the fourth harmonic generator is highly polarized. We used a dichroic mirror to remove the fundamental light and the frequency doubled light (generated in the process of frequency quadrupling) prior to the wave plate. The sets of images presented in this report are typically acquired in 24 minutes to gain a sufficient signal-to-noise ratio, such that the area of interest is reasonably resolved after the data processing. We show the measurement geometry with respect to the sample in Fig. 3 (a).

RESULTS:

We tested the automated polarization-controlled data acquisition using dielectric stacks comprised of an Al_2O_3 overlayer, SiO_2 underlayer, and Si substrate as reference samples. We have chosen dielectric stacks because they exhibit strong polarization-dependent light absorption in the DUV wavelength range as described in the following paragraph. In order to examine the impact of subtle changes in optical constraints, dielectric stacks encapsulate atomically-thin

MoS$_2$ flakes. Layers of MoS$_2$ are only three-atoms thick, making detection of buried MoS$_2$ layers an excellent test for detecting the subtle differences in optical constants with respect to the surrounding dielectrics. Atomically-thin MoS$_2$ flakes (mostly monolayer specimens, with some multilayer regions near the center of the flakes) were grown on Si wafers covered with 100-nm-thick SiO$_2$ [I. Bilgin, et al., Chemical Vapor Deposition Synthesized Atomically Thin Molybdenum Disulfide with Optoelectronic-Grade Crystalline Quality, ACS Nano, 2015, 9 (9), pp 8822–8832]. We then covered the entire sample surface with Al$_2$O$_3$ overlayers via atomic layer deposition [D. M. Hausmann, et al., Atomic Layer Deposition of Hafnium and Zirconium Oxides Using Metal Amide Precursors, Chem. Mater., 2002, 14 (10), pp 4350–4358]. The conformal geometry of the Al$_2$O$_3$ films was verified using atomic force microscopy. We verified the thicknesses of Al$_2$O$_3$ overlayers using optical ellipsometry in the wavelength range of 400 to 1200 nm. Thus, MoS$_2$ flakes are encapsulated between SiO$_2$ and Al$_2$O$_3$ films, as illustrated in Fig. 3 (a).

In Fig. 3 (b) to (d), we show calculated optical absorption as a function of wavelength and Al$_2$O$_3$ overlayer thickness for (b) TE- and (c) TM-polarized and (d) unpolarized incident light. The white dash lines indicate the wavelength of the λ=210nm ultrafast pulsed laser. Most importantly, calculated optical absorption at λ=210nm (along the white dash lines) varies from low, high, to low for TE-polarized incident light for increasing Al$_2$O$_3$ overlayer thickness (Fig. 3 (b)), while it varies high, low, to high for the TM-polarized incident light. Black markers with white circumferences depict the thicknesses of Al$_2$O$_3$ overlayer for the three samples measured in this study (shown in Fig. 4). We selected the thicknesses of the Al$_2$O$_3$ overlayer to lie close to the extrema of the calculated optical absorption. This result indicates that the polarization-dependent photoemission yield measurement is expected to display significant differences between TE- and TM-polarized light among the three samples.

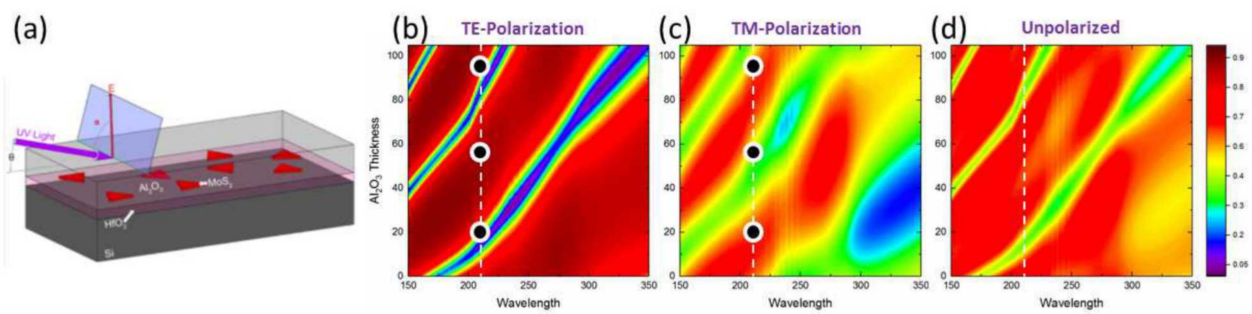

Figure 3 (a) Schematic illustration of the dielectric stack with embedded monolayer MoS2 flakes and the geometry of light illumination with polarization vector controlled by the automated data acquisition. The dielectric stacks consist of 100 nm-thick SiO2 underlayer and varying thickness of Al$_2$O$_3$ overlayer sandwiching the MoS2 flakes. We performed DUV-PEEM using linearly polarized light incident at an angle 16° relative to the surface parallel. (b) Calculated absorption as a function of wavelength and Al$_2$O$_3$ overlayer thickness for (b) TE- and (c) TM-polarized and (d) unpolarized incident light. Black markers with white circumferences are the thicknesses of Al$_2$O$_3$ overlayer for the three samples shown in Fig. 4.

As predicted by the calculated optical absorption, the polarization-dependent photoemission yield of the dielectric stacks displayed significant variations between TE- and TM-polarized illuminations. In Fig. 4, we show the polarization-dependent photoemission yield measured using DUV-PEEM as a function of the orientation of the linear polarization. The reference for the polarization angle is illustrated in Fig. 3 (a): α=0 depicts that the orientation of the light polarization is fully in-plane of the sample surface, thus TE-polarization (i.e. s-polarization). α=90 depicts that the orientation of the light polarization is fully out-of-plane of the sample surface, thus TM-polarization (i.e. p-polarization). For the Al_2O_3 overlayer thickness of 19 nm (Fig. 4 (a)) and 93 nm (Fig. 4 (c)), photoemission yield is much stronger for TE-polarization than for TM-polarization due to high optical absorption, illustrated by the peanut-shape trace lying horizontally. On the contrary, the 56 nm-thick Al_2O_3 overlayer displayed stronger absorption for TM-polarization, resulting in the vertical peanut-shape trace (Fig. 4 (b)). The calculation using the transfer matrix method to model Fabry-Pérot interference closely predicted these polarization dependences as illustrated by the red lines in Fig. 4. Overall, the measurements of polarization-dependent photoemission yield illustrate the sensitivity of the measurement to the optical properties, or optical constants, of the cavities formed by the dielectric stacks.

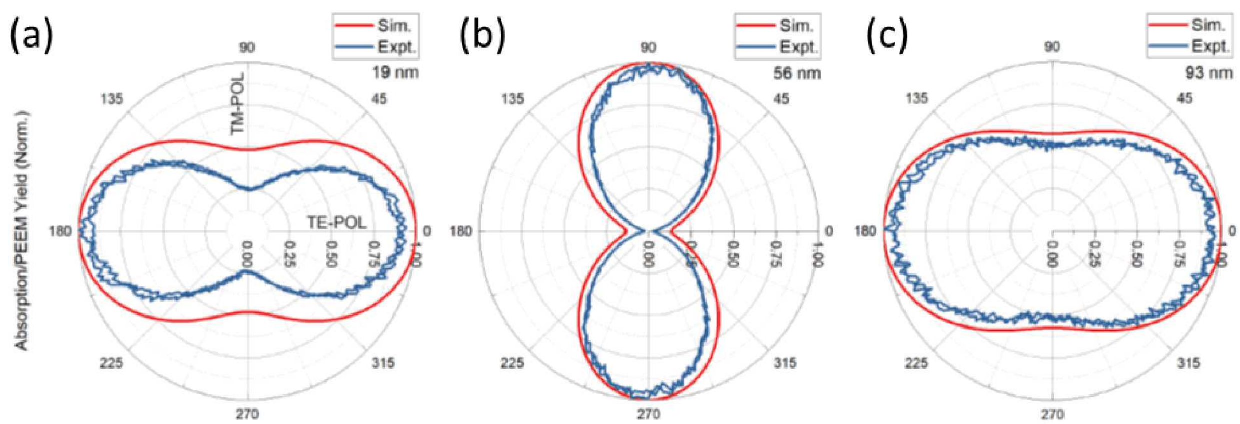

Figure 4 Normalized DUV-PEEM yield and predicted absorption for samples with overlayers of Al_2O_3 having thicknesses of (a) 19, (b) 56, and (c) 93 nm.

We further exploited the sensitivity of polarization-dependent photoemission yield to image the encapsulated atomically-thin MoS_2 flakes. We took an approach to fit the polarization-dependent photoemission yield data as described in the following. In Fig. 5 (a), we show a typical polarization-dependent photoemission intensity plotted as a function of the waveplate angle, where one rotation of the waveplate yields four oscillating cycles of the photoemission intensity. Conversion of the waveplate angle to the orientation of the linear polarization yields the peanut-shape trace shown in Fig. 4. We fitted these oscillating cycles of the photoemission intensity using a sinusoidal function with an offset, which results in 3 fitting parameters: the intensity amplitude, the average intensity, and the polarization angle offset as illustrated in Fig. 5 (a). In Fig. 5 (b) to (c), we show the spatial maps of two out of three fitting parameters providing an impressive level of detail for the MoS_2 flakes encapsulated by 93 nm-thick Al_2O_3. The dataset proves that the polarization-dependent PEEM imaging is capable of detecting the subtle difference in the optical properties of the dielectric cavity by the insertion of the MoS_2 flakes.

In essence, this visualization scheme is equivalent to ellipsometry imaging leveraging the local variation of the optical constants. The absence of variation for the polarization angle offset shown in Fig. 5 (d) further supports that the spatial variation of the optical constants is not large in magnitude. Detailed optical modeling of the image formation is underway. We note that, for the image contrast mechanisms that involve the atomic or molecular alignment or magnetic domains, we anticipate a larger spatial variation in the polarization angle offset.

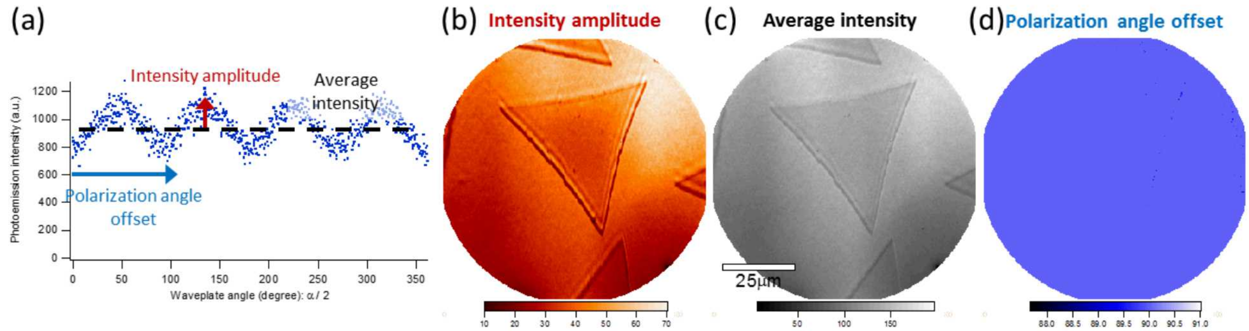

Figure 5 (a) A typical polarization-dependent photoemission intensity plotted as a function of the waveplate angle, illustrating the definitions of intensity amplitude, average intensity, and polarization angle offset used as fitting parameters. (b) to (d) The spatial maps of the intensity amplitude, average intensity, and polarization angle offset obtained from the fitting process. The dielectric stack consists of 100nm-thick SiO_2 and 93 nm-thick Al_2O_3.

ANTICIPATED OUTCOMES AND IMPACTS:

The capability development accomplished through this project has far-reaching implications for a number of Research Challenges at SNL and for an existing program. Magnetic imaging with high spatial resolution is sought after for evaluating spintronics, which is an emerging element for the Beyond Moore Research Challenge and the Trusted Systems & Communications Research Challenge. The knowledge of magnetic behaviors is one of the fundamental aspects for quantum materials and nano science, and an important factor for controlling variability of magnetic materials for real-world applications. The results from this project thus align well with the Engineering of Materials' Reliability Research Challenge. It is also anticipated to benefit the Center for Integrated Nanotechnologies (CINT) supported by the DOE Office of Science through magnetic studies of nano materials, where high spatial resolution is desired.

Throughout this project in FY17, we had identified three major possible improvements: (1) replacing the deep UV pulsed laser with a state-of-the-art commercially available CW laser reaching 10 to 100mW, (2) replacing the refocusing optics to eliminate the non-uniform laser beam profile at the sample position, and (3) modifying the data acquisition software to be able to shorten the data accumulation time per image and the total data acquisition time to improve the image statistics. The third possible improvement was completed in FY18 supported by the continuation of this project. We plan to achieve the first and second improvements using the new CW laser in FY19 supported by CINT user program.

Beside the three potential improvements outlined in the previous paragraph, the next major goal is to realize the coincident-site FM and aFM imaging by switching the illuminating light between circular and linear polarizations. Realization of such a scientific study would make an invaluable contribution toward understanding the ferromagnetic/anti-ferromagnetic interfaces and developing spintronics applications.

CONCLUSION:

We present the development of polarization-dependent PEEM imaging using deep UV light based on λ=213nm pulsed laser in this report. We applied the newly-developed automated polarization-dependent photoemission yield measurement to dielectric stacks with MoS_2 flake inclusions, and demonstrated ellipsometry imaging of the buried MoS_2 flakes using this PEEM-based imaging approach. Together with the in-plane and out-of-plane ferromagnetic imaging accomplished in FY17, the results presented here support the notion of magnetic imaging using deep UV magnetic circular dichroism and magnetic linear dichroism PEEM as a viable approach to examine a broad range of magnetic materials and spintronic devices.

Sandia National Laboratories is a multimission laboratory managed and operated by National Technology and Engineering Solutions of Sandia LLC, a wholly owned subsidiary of Honeywell International Inc. for the U.S. Department of Energy's National Nuclear Security Administration under contract DE-NA0003525.